NUCLEAR SCIENCE AND TECHNIQUES **26**, 030507 (2015)

TiO_2 nanofilm growth by Ti ion implantation and thermal annealing in O_2 atmosphere*

ZHOU Xiao-Dong (周小东),† ZHOU Si-Hua (周思华), SUN Xian-Ke (孙现科), and ZHANG Yun-Li (张云丽)
School of Physics and Electromechnical Engineering, Zhoukou Normal University, Zhoukou 466001, China
(Received March 13, 2015; accepted in revised form April 19, 2015; published online June 20, 2015)

TiO_2 nanofilms on surface of fused silica were fabricated by Ti ion implantation and subsequent thermal annealing in oxygen ambience. The silica glasses were implanted by 20 kV Ti ions to 1.5×10^{17} ions/cm^2 on an implanter of metal vapor vacuum arc (MEVVA) ion source. Effects of annealing parameters on formation, growth and phase transformation of the TiO_2 nanofilms were studied in detail. Optical absorption spectroscopy, Raman scattering spectroscopy, X-ray photoelectron spectroscopy, scanning electron microscopy and transmission electron microscopy measurements were done to figure out formation mechanism of the TiO_2 nanofilms. The formation of TiO_2 nanofilms was due to out-diffusion of the implanted Ti ions to the substrate surface, where they were oxidized into TiO_2 nanoparticles. Formation, phase, and thickness of the TiO_2 nanofilms can be well tailored by controlling annealing parameters.

Keywords: Ion implantation, Thermal annealing, TiO_2 nanofilms, Characterization

DOI: 10.13538/j.1001-8042/nst.26.030507

I. INTRODUCTION

Since TiO_2-photoassisted electro-chemical water splitting was reported by Honda and Fujishima in 1972 [1], titanium oxides have attracted much attention due to their wide applications, such as photocatalysis for environmental treatments and hydrogen production, dye-sensitized solar cells for photovoltaics, sensors, smart windows, and display devices, etc. [2–5]. Conventional TiO_2 powder catalysts are disadvantageous in the needs of stirring in the reaction and separation (after reaction). TiO_2 thin films make it possible to overcome the disadvantages and extend industrial applications. A variety of techniques were used to prepare TiO_2 thin films, including sol gel processing [6], spray pyrolysis [7, 8], magnetron sputtering [9], and chemical vapor deposition [10]. Photocatalytic TiO_2 films prepared by wet chemistry process (e.g., sol gel method) show good photocatalytic performance, but their mechanical durability is not good enough for practical applications such as self-cleaning glasses for window and automotive mirror. In addition, they are generally inferior for applications requiring large area films [11]. While applications of these TiO_2 films are limited due to their unsatisfactory stability and reliability, TiO_2 films fabricated by physical methods generally have higher film adhesion and stability for practical uses [12].

Nanomaterials, nanoparticles and nanofilms can be fabricated by ion implantation. Metal oxide semiconductors are produced by a solid phase growth process of metal ion implantation and subsequent thermal oxidation, such as ZnO [13–16] or TiO_2 [17, 18] nanomaterials by Zn or Ti ion implantation. Nanofilms made by ion implantation, due to their formation under high temperatures, usually show good adhesion and stability. In this paper, TiO_2 nanofilms in the solid phase growth process of Ti ion implantation are formed into fused silica substrate and subsequent thermal annealing in oxygen ambience. Effects of the implantation and annealing parameters on the formation, phase and growth of the TiO_2 nanofilms are studied, so as to understand mechanisms of TiO_2 nanofilm formation. The nanofilm thickness and phase can be well tailored by controlling the implantation and annealing parameters.

II. EXPERIMENTAL

A. Sample preparation

High purity silica slides (20 mm × 20 mm × 1 mm) were implanted by 20 kV Ti ions to 1.5×10^{17} ions/cm^2 on an implanter of metal vapor vacuum arc (MEVVA) ion source. The samples were kept rotating in a horizontal plane during ion implantation, with the sample holder being cooled by circulating water. The implanted samples were annealed under O_2 atmosphere in a conventional tube furnace. Group 1 of the samples were annealed for 2 h at 500 °C, 600 °C, 700 °C, 800 °C, 900 °C and 1000 °C. Group 2 were annealed at 800 °C for 2, 4 and 6 h.

B. Sample characterization

Optical absorption spectra of the samples were measured on a UV-vis-NIR dual-beam spectrophotometer (Varian Cary5000) in wavelength range of 200–800 nm. Surface morphologies of the implanted samples before and after thermal annealing were examined by using a scanning electron microscopy (SEM, FEI Sirion). Raman scattering spectra were measured using a micro-Raman microscope (Jobin-Yvon LabRAM HR) equipped with a cooled CCD detector under a backscattering geometry to identify the crystalline phase of TiO_2. The excitation source was the blue line (488 nm) of an Ar^+ laser powered at 5 mW, with its scan den-

* Supported by National Natural Science Foundation of China (No. 11405280), Foundation from Education Department of Henan Province (No. 14B140021) and the Startup Foundation for Doctors of Zhoukou Normal University (No. zksybscx201210)
† Corresponding author, zhouxd516@163.com

sity varying from 100 to 1200 cm^{-1}. Microstructural characterization of the as-implanted and annealed samples was performed on a JEOL 2010 (HT) transmission electron microscope (TEM) operated at 200 kV. X-ray photoelectron spectroscopy (XPS) analysis was done on a Kratos XSAM800 XPS system with Mg K_α (1253.6 eV) as the radiation source under a vacuum of 6×10^{-7} Pa.

III. RESULTS AND DISCUSSION

A. Optical absorption spectra of Ti ions implanted samples versus annealing temperature

Figure 1 shows optical absorption spectra of the as-implanted sample and the samples annealed for 2 h at 500–1000 °C. In the absorption spectra of the as-implanted sample, the background absorption increases drastically in the UV and visible regions. This is due to absorption of implantation-induced point defects and the Ti nanoparticles formed in silica substrate. Annealed at 500 °C, the background absorption reduces drastically due to the defect annihilation by thermal annealing. Also, an abrupt absorption edge appears, due to presence of anatase TiO_2 [19, 20], which was formed upon post-implantation annealing at 500 °C. For all the annealed samples, the spectra present a trend that the absorption edges shift to longer wavelength with the increase of annealing temperature, implying an increase in mean sizes of the TiO_2 nanoparticles. It is interesting to note that the sample annealed at 1000 °C differs obviously from other annealed samples in spectrum with a greater shift of absorption edge to longer wavelength. This remarkable shift of absorption edge suggests that phase transformation of TiO_2 from anatase to rutile may occur at 1000 °C. Such shifts of the maximum absorption and absorption edge induced by the phase transformation are similar to the results in Refs. [20, 21].

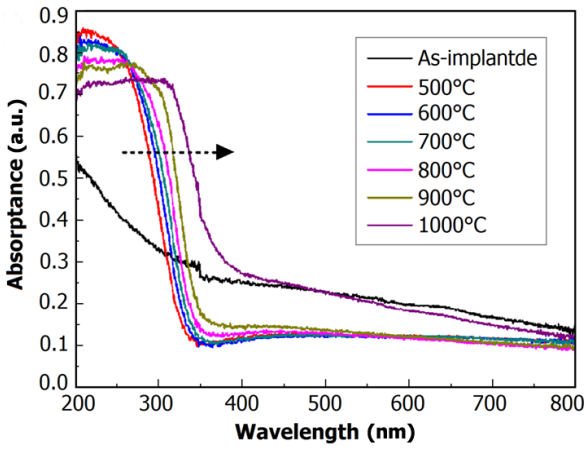

Fig. 1. (Color online) Optical absorption spectra of samples implanted to 1.5×10^{17} Ti ions/cm^2 and annealed at 500–1000 °C for 2 h.

B. SEM images of Ti ions implanted samples versus annealing temperature

Surface morphologies of the samples were investigated by SEM. Figure 2 shows the SEM images of the Ti ions implanted samples annealed for 2 h at 500, 600, 700, 800, 900 and 1000 °C.

On the whole, the surface morphology changes obviously for the samples annealed at different temperatures. At 500 °C, some small-sized nanoparticles began to appear, indicating the TiO_2 nanoparticles formed at 500 °C. At 600 °C, a smooth and homogenous film was formed, with many near-spherical nanoparticles distributed compactly on the substrate surface. The sizes of TiO_2 nanopartices increase with the annealing temperature, with the mean diameter of particles being 25.3, 37.6 and 45.8 nm at 600 °C, 700 °C and 800 °C, respectively. At 900 °C, however, the TiO_2 nanoparticles in the surface aggregated and formed cross-linked particles of about 61.4 nm in diameter, as shown in Fig. 2(e). The surface morphology underwent a big change at 1000 °C, and the TiO_2 nanoparticles in the substrate surface became embedded and undistinguished, as shown in Fig. 2(f).

Interestingly, evolution of surface morphologies of the samples as a function of annealing temperature in Fig. 2 is well related with the results from optical absorption spectra (Fig. 1). The increase in both the particle size and crystal quality as a function of annealing temperature leads to the absorption edge shift towards longer wavelength. The abrupt shift of absorption edge observed at 1000 °C is just a result of structure change characterized by SEM, and the change may be due to the phase transformation from anatase to rutile.

C. Formation and phase of TiO_2 nanocrystals: Raman scattering spectroscopy and XPS measurements

The Raman spectroscopy measurements were made to identify and analyze the formation and phase of TiO_2 nanocrystals after thermal annealing. Figure 3 shows Raman spectra of the bare silica, the as-implanted sample and the Ti ions implanted samples annealed for 2 h at 500–1000 °C. Some Raman peaks of SiO_2 can be observed in the bare silica sample. However, Raman spectrum of the as-implanted silica became almost featureless due to extensive structural damage induced by ion implantation. The structure of silica is partially recovered by subsequent thermal annealing, and the Raman peaks of SiO_2 in the annealed samples can be observed again. A Raman peak centered at about 140 cm^{-1} appears at 600 °C. This can be assigned as E_g mode of TiO_2 in anatase phase [22, 23]. The Raman peak height increases with temperature from 600 °C to 900 °C, indicating the increased crystallinity and amount of the anatase phase TiO_2. However, for the sample annealed at 1000 °C, the spectrum shape changed, with three Raman peaks centered at 605, 440 and 230 cm^{-1}. These can be ascribed to the two-phonon scattering of A_{1g} and E_g modes, and the second-order effect of the rutile phase TiO_2, respectively [24]. Thus, the anatase-to-

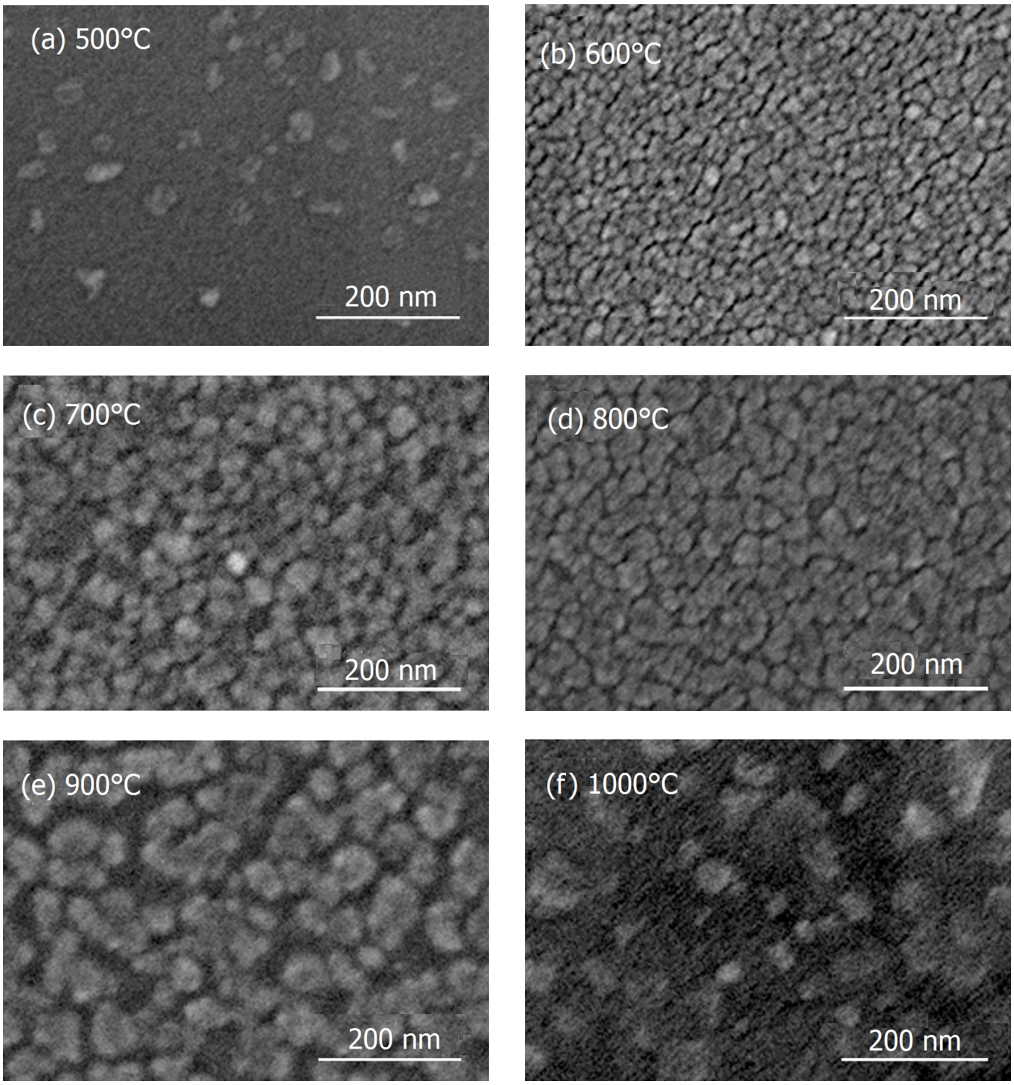

Fig. 2. SEM images of the samples implanted to 1.5×10^{17} Ti ions/cm^2 and annealed for 2 h at 500–1000 °C.

rutile phase transformation taking place at the high temperature is confirmed.

The formation and evolution of the anatase phase in the annealed samples is consistent with the evolution of optical absorption spectra in Fig. 1 and SEM in Fig. 2. The increase in size and crystal quality of the nanoparticles as a function of annealing temperature leads to the red-shift of the absorption edge and the intensification of the E_g Raman mode. However, the absorption edge of TiO_2 in the sample annealed at 500 °C was observed, while the crystalline phase in the same sample was not detected by Raman spectroscopy. It is well known that optical absorption spectrum usually gives average structural information, whereas Raman scattering spectrum as a local probe is sensitive to crystallinity and microstructures of materials. That the Raman peaks could not observed implies that annealing at lower temperatures produced not enough TiO_2 nanocrystals, which can be verified by the SEM image in Fig. 2(a). Also, the nanocrystals are not of good crystallinity, though the absorption edges of TiO_2 were confirmed by optical absorption measurement.

By carefully analyzing the change of E_g modes centered at 140 cm^{-1} of the anatase phase TiO_2 as a function of annealing temperature, we found that the intensity, frequency and linewidth (FWHM) of the E_g Raman mode are strongly dependent on the annealing treatment. The linewidth of Raman peaks indicates that the TiO_2 nanofilms are of high crystallinity. The intensity of E_g Raman mode increases with annealing temperature, accompanied by a downshift in frequency and a decrease in linewidth. The sample annealed at 900 °C exhibits a large downshift in frequency and an obvious decrease in the linewidth. A similar behavior of frequency shift and linewidth decrease of E_g Raman mode was observed in TiO_2 nanoparticles fabricated by other methods [24–28].

Mechanisms proposed to interpret this behavior include the phonon confinement effect [24, 29], internal stress/surface tension effects [28, 30], and nonstoichiometry due to oxy-

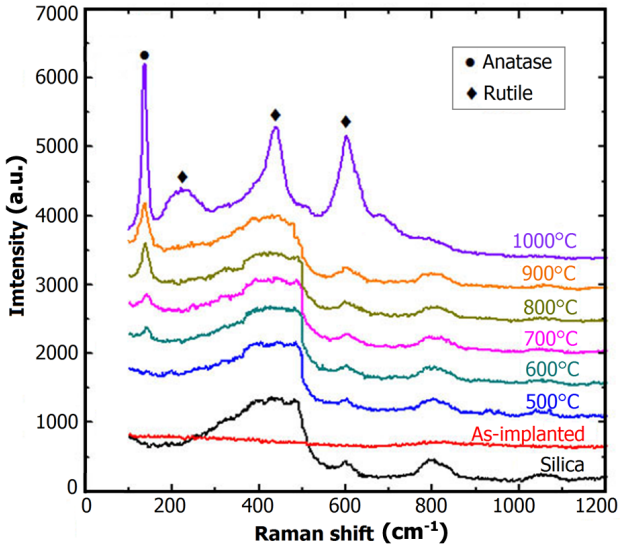

Fig. 3. (Color online) Raman spectra of bare silica, the 1.5×10^{17} Ti ions/cm^2 as-implanted sample, and annealed for 2 h at 500–1000 °C.

gen deficiency [25, 26]. The pressure effect mechanism usually leads to large frequency shifts, and Raman measurements as a function of the external pressure shows that the Raman modes undergo a downshift in frequency with increasing pressure [31]. For instance, the pressure effect induced by the surrounding particles or the interface stress has been successfully used to elucidate the frequency shift of the Raman peaks observed in TiO_2 and $PbTiO_3$ nanoparticles [32]. The size-induced pressure effect may act in a manner similar to an external pressure on the TiO_2 nanoparticles. The smaller the nanoparticles are, the larger the contribution of pressure is, hence the frequency downshift of the E_g annatase mode [28].

In our experiment, the size of TiO_2 nanoparticles increases with annealing temperature, and the pressure releases gradually with heat treatment, which can lead to the frequency upshift (towards to higher frequency) of the E_g mode according to the size-induced pressure effect. However, instead of upshift, a frequency downshift with increasing annealing treatment was observed, implying that the pressure effect can be ruled out. In addition, according to the phonon confinement effects, the increase in crystallite size can cause downshift in frequency and decrease in linewidth of the E_g Raman mode, thus the phonon confinement effects should be taken into account to explain the change of E_g Raman mode.

Also, non-stoichiometry observed in nanophase TiO_2 samples prepared by other methods [24–26] plays an important role in frequency shift of Raman peaks, in which the frequency downshifts with decreasing oxygen deficiency. Although the TiO_2 samples used in this work are prepared by Ti-ion implantation and subsequent annealing in an oxygen atmosphere, oxygen deficiency, as the most common form of nonstoichiometry in TiO_2, can not be ruled out. Moreover, the downshift in frequency of the E_g annatase mode with increasing annealing temperature (the decrease of oxygen deficiency) is well consistent with the results reported by other authors [24–26]. The oxygen defiency decreases with increasing annealing temperature. Therefore, the nonstoichiometry should be taken into account in explaining changes in the E_g Raman mode in our TiO_2 films.

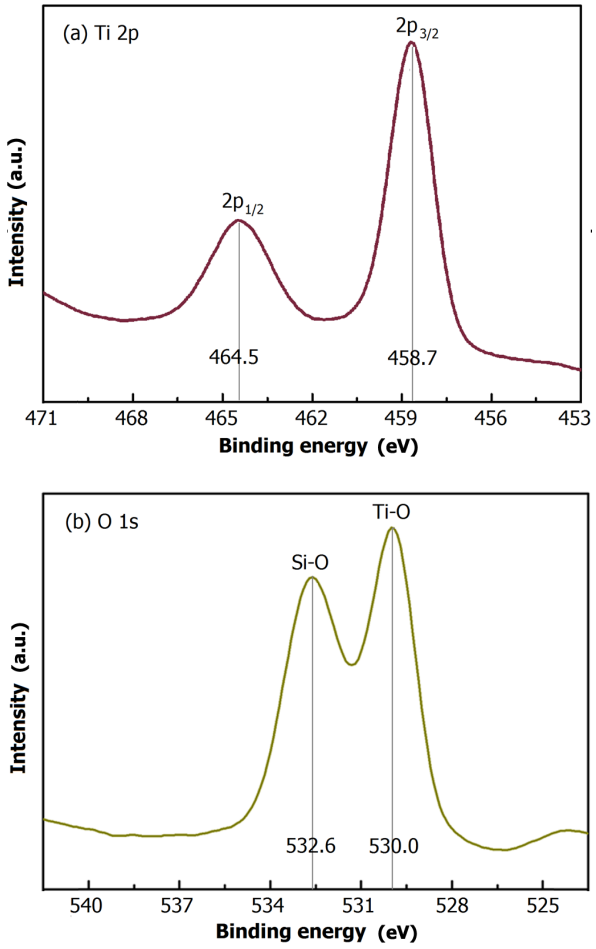

Fig. 4. (Color online) XPS Ti 2p (a) and O 1s (b) core-level spectra of the 1.5×10^{17} Ti ions/cm^2 implanted sample and annealed at 800 °C.

To further confirm the formation of TiO_2 nanofilms and measure the atomic ratio of Ti and O, the XPS spectra of the implanted samples annealed at 800 °C was measured (Fig. 4). The peaks centered at 458.7 eV and 464.5 eV binding energies correspond to the $2p$ 3/2 and 1/2 core levels of Ti^{4+}, and the peaks centered at 530.0 eV and 532.6 eV correspond to the binding energies of Ti-O and Si-O, respectively, agreeing well with the values reported by other authors [3]. The atomic ratio of Ti and O was calculated as 1 : 1.82, proving the nonstoichiometry of TiO_2. The color of the annealed samples changes from light-blue to almost white at 900 °C, indicating a decrease in oxygen vacancies [30] and a change of films thicknesses according to interference phenomena in thin films.

D. Mechanism for the formation of TiO_2 nanofilms: TEM Characterization

To figure out growth process and formation mechanism of the TiO_2 nanofilms, the TEM study on microstructure of the samples was carried out. Figure 5 shows the cross sectional TEM images of the as-implanted sample and the sample annealed at 800 °C for 2 h. A dark layer with tiny Ti nanocrystals below the surface was observed in the as-implanted sample (Fig. 5(a)). After annealing at 800 °C for 2 h, a nanofilm in thickness of 10 nm was formed on the sample surface (Fig. 5(b)). The selected area electron diffraction (SAED) pattern confirms the formation of an anatase phase TiO_2 nanofilm. Meanwhile, the Ti atoms in the silica substrate aggregate into larger nanocrystals according to the SAED pattern. This indicates that during annealing in O_2 atmosphere, the implanted Ti atoms diffused out to the silica surface and were oxidized into TiO_2 nanoparticles. Meanwhile, the embedded Ti nanocrystals form larger ones due to the Ostwald ripening effect.

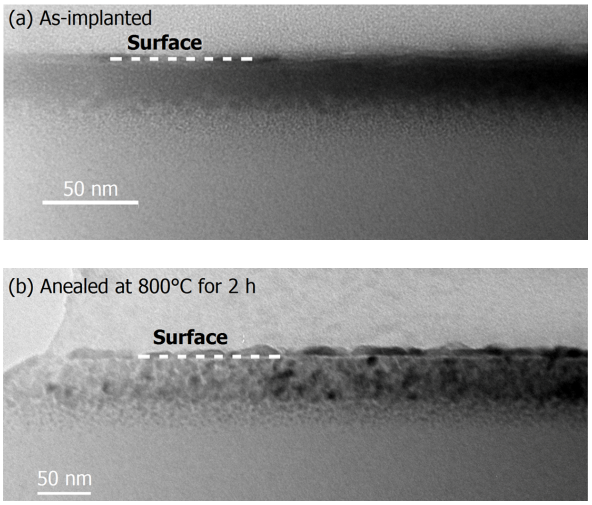

Fig. 5. Cross sectional TEM images of the 1.5×10^{17} Ti ions/cm^2 as-implanted sample (a) and sample annealed at 800 °C for 2 h(b).

The solid phase growth process of TiO_2 nanofilms by ion implantation and subsequent thermal oxidation is similar to the results reported on Zn-implanted silica and sapphire to form high-quality ZnO nanofilms on the substrate surface [14–16]. The formation of metal oxide semiconductor by metal ion implantation and subsequent thermal oxidation was due to out-diffusion of the implanted Ti ions to the substrate surface, where they were oxidized into TiO_2.

E. Growth of the TiO_2 nanofilms: Influence of the annealing time

The annealing time was increased to 4 h and 6 h, so as to further study the growth process and formation mechanism of the TiO_2 nanofilms. The cross sectional TEM images of

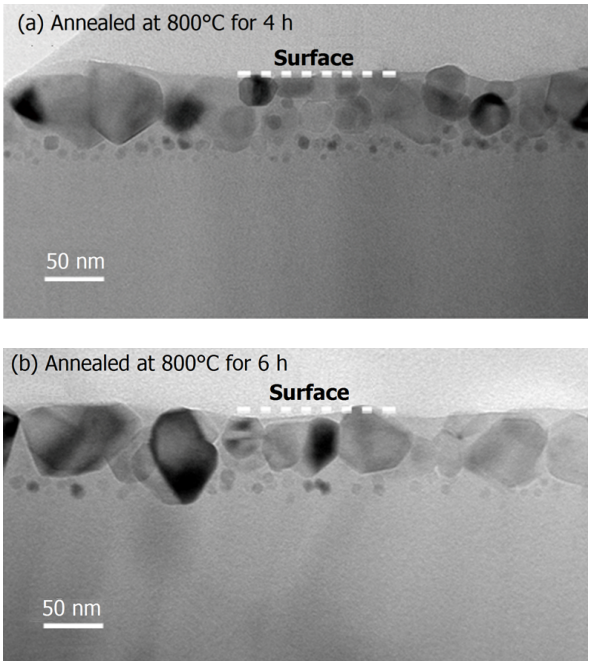

Fig. 6. Cross sectional TEM images of the 1.5×10^{17} Ti ions/cm^2 implanted samples and samples annealed at 800 °C for 4 h (a) and 6 h (b).

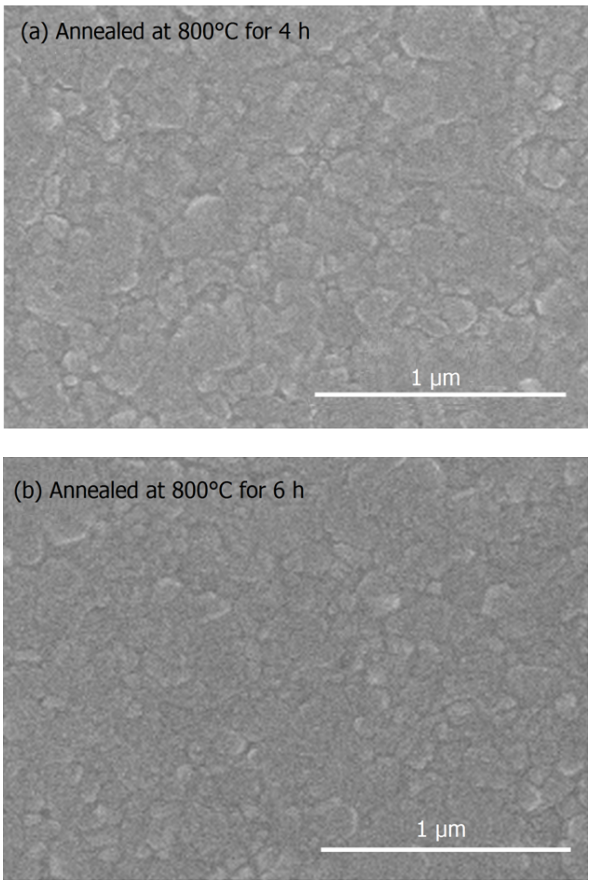

Fig. 7. SEM images of the 1.5×10^{17} Ti ions/cm^2 implanted samples annealed at 800 °C for 4 h (a) and 6 h (b).

the Ti ions implanted samples annealed at 800 °C for 4 h and 6 h are shown in Fig. 6. In Fig. 6(b), almost all the Ti atoms diffused out of the substrate to form a thicker TiO_2 nanofilm with a thickness of 50 nm, and the TiO_2 nanocrystals increased greatly in size. It should be mentioned that the TiO_2 nanofilms have a slow growth rate of about 0.15 nm/min to ensure the high crystal quality and high density of the formed nanofilms. Figure 7 shows SEM images of the samples annealed at 800 °C for 4 h and 6 h. The film of 6-h annealing has flatter film surface and larger nanocrystal size than the film of 4-h annealing.

Combining the TEM with SEM results, annealing time was expected to affect the surface morphology, structure and thickness of the formed TiO_2 nanofilms when the samples were annealed at 800 °C. Thickness of TiO_2 nanofilms increases with annealing time until all of the Ti atoms diffuse out of the substrate to form a thicker TiO_2 nanofilm. As discussed above, the absorption edge and phase transformation of TiO_2 are annealing temperature dependent, and the thickness of the TiO_2 nanofilms is annealing time dependent.

IV. CONCLUSION

In summary, TiO_2 nanofilms were fabricated on fused silica substrate by a solid phase growth process of Ti-ion implantation and subsequent thermal annealing in an O_2 atmosphere. The growth mechanism and phase transformations of TiO_2 nanofilms were discussed. The grain sizes and the crystallographic phase of TiO_2 nanofilms can be tailored. A higher annealing temperature produced a larger nanograin size, and the anatase-to-rutile phase transformation occurred at annealing temperatures higher than 1000 °C. The thickness of the TiO_2 nanofilms is annealing time dependent, and it is determined by all of the Ti atoms which diffuse out of the substrate to form a thicker TiO_2 nanofilms through subsequent thermal annealing under O_2 atmosphere. Thus, the formation, phase and growth of the TiO_2 nanofilms can be well tailored by controlling the annealing parameters (temperature and time). The results indicate that the TiO_2 nanofilms fabricated by this approach have great potential for various optical, sensing and catalytic applications.

[1] Fujishima A and Honda K. Electrochemical Photolysis of Water at a Semiconductor Electrode. Nature, 1972, **238**: 37-38. DOI:10.1038/238037a0

[2] Fröschl T, Hörmann U, Kubiak P, *et al*. High surface area crystalline titanium dioxide: potential and limits in electrochemical energy storage and catalysis. Chem Soc Rev, 2012, **41**: 5313–5360. DOI: 10.1039/c2cs35013k

[3] Chen X B and Mao S S. Titanium dioxide nanomaterials: synthesis, properties, modifications, and applications. Chem Rev, 2007, **107**: 2891–2959. DOI: 10.1021/cr0500535

[4] Liang F X, Kelly T L, Luo L B, *et al*. Self-cleaning organic vapor sensor based on a nanoporous TiO_2 interferometer. ACS Appl Mater Interfaces, 2012, **4**: 4177–4183. DOI: 10.1021/am300896p

[5] Song Y Y, Gao Z D, Wang J H, *et al*. Multistage coloring electrochromic device based on TiO_2 nanotube arrays modified with WO_3 nanoparticles. Adv Funct Mater, 2011, **21**: 1941–1946. DOI: 10.1002/adfm.201002258

[6] Choi H, Stathatos E and Dionysiou D D. Sol-gel preparation of mesoporous photocatalytic TiO_2 films and TiO_2/Al_2O_3 composite membranes for environmental applications. Appl Catal B-Environ, 2006, **63**: 60-67. DOI: 10.1016/j.apcatb.2005.09.012

[7] Stambolova I, Shipochka M, Blaskov V, *et al*. Sprayed nanostructured TiO_2 films for efficient photocatalytic degradation of textile azo dye. J Photoch Photobio B, 2012, **117**: 19–26. DOI:10.1016/j.jphotobiol.2012.08.006

[8] Stambolova I, Blaskov V, Shipochka M, *et al*. Effect of post-synthesis acid activation of TiO_2 nanofilms on the photocatalytic efficiency under visible light. J Phys Conf Ser, 2014, **558**: 012055. DOI:10.1088/1742-6596/558/1/012055

[9] Casu M B, Braun W, Bauchspiess K R, *et al*. A multi-technique investigation of TiO_2 films prepared by magnetron sputtering. Surf Sci, 2008, **602**: 1599–1606. DOI: 10.1016/j.susc.2008.02.030

[10] Sun H F, Wang C Y, Pang S H, *et al*. Photocatalytic TiO_2 films prepared by chemical vapor deposition at atmosphere pressure. J Non-Cryst Solids, 2008, **354**: 1440–1443. DOI: 10.1016/j.jnoncrysol.2007.01.108

[11] Yu J G and Zhao X J. Effect of substrates on the photocatalytic activity of nanometer TiO_2 thin films. Mater Res Bull, 2000, **35**: 1293–1301. DOI: 10.1016/S0025-5408(00)00327-5

[12] Kleiman A, Márquez A, Vera M L, *et al*. Photocatalytic activity of TiO_2 thin films deposited by cathodic arc. Appl Catal B-Environ, 2011, **101**: 676–681. DOI:10.1016/j.apcatb.2010.11.009

[13] Amekura H, Umeda N, Sakuma Y, *et al*. Fabrication of ZnO nanoparticles in SiO_2 by ion implantation combined with thermal oxidation. Appl Phys Lett, 2005, **87**: 013109. DOI: 10.1063/1.1989442

[14] Ren F, Jiang C Z and Xiao X H. Fabrication of single-crystal ZnO film by Zn ion implantation and subsequent annealing. Nanotechnology, 2007, **18**: 285609. DOI:10.1088/0957-4484/18/28/285609

[15] Xiao X H, Ren F, Fan L X, *et al*. ZnO single-crystal films fabricated by the oxidation of zinc-implanted sapphire. Nanotechnology, 2008, **19**: 325604. DOI:10.1088/0957-4484/19/32/325604

[16] Liu Y X, Liu Y C, Shao C L, *et al*. Excitonic properties of ZnO nanocrystalline films prepared by oxidation of zinc-implanted silica. J Phys D Appl Phys, 2004, **37**: 3025–3029. DOI:10.1088/0022-3727/37/21/013

[17] Xiang X, Chen M, Ju Y F, *et al*. N–TiO_2 nanoparticles embedded in silica prepared by Ti ion implantation and annealing in nitrogen. Nucl Instrum Meth B, 2010, **268**: 1440–1445. DOI: 10.1016/j.nimb.2010.01.023

[18] Ren F, Zhou X D, Liu Y C, *et al*. Fabrication and properties of TiO_2 nanofilms on different substrates by a novel and universal method of Ti-ion implantation and subsequent annealing. Nanotechnology, 2013, **24**: 255603. DOI:10.1088/0957-4484/24/25/255603

[19] Asahi R, Morikawa T, Ohwaki T, *et al*. Visible-light photocatalysis in nitrogen-doped titanium oxides. Science, 2001, **293**: 269–271. DOI: 10.1126/science.1061051

[20] Zhang J, Li M J, Feng Z C, *et al*. UV Raman spectroscopic study on TiO_2. I. phase transformation at the surface and in the bulk. J Phys Chem B, 2006, **110**: 927–935. DOI: 10.1021/jp0552473

[21] Bickley R I, Gonzalez-Carreno T, Lees J S, *et al*. A structural investigation of titanium dioxide photocatalysts. J Solid State Chem, 1991, **92**: 178–190. DOI: 10.1016/0022-4596(91)90255-G

[22] Ohsaka T, Izumi F and Fujiki Y. Raman spectrum of anatase TiO_2. J Raman Spectrosc, 1978, **7**: 321–324. DOI: 10.1002/jrs.1250070606

[23] Chaves A, Katiyan K S and Porto S P S. Coupled modes with A1 symmetry in tetragonal $BaTiO_3$. Phys Rev B, 1974, **10**: 3522–3533. DOI: 10.1103/PhysRevB.10.3522

[24] Zhang W F, He Y L, Zhang M S, *et al*. Raman scattering study on anatase TiO_2 nanocrystals. J Phys D Appl Phys, 2000, **33**: 912–916. DOI:10.1088/0022-3727/33/8/305

[25] Parker J C and Siegel R W. Raman microprobe study of nanophase TiO_2 and oxidation-induced spectral changes. J Mater Res, 1990, **5**: 1246–1252. DOI: 10.1557/JMR.1990.1246

[26] Parker J C and Siegel R W. Calibration of the Raman spectrum to the oxygen stoichiometry of nanophase TiO_2. Appl Phys Lett, 1990, **57**: 943–945. DOI: 10.1063/1.104274

[27] Bersani D, Lottici P P and Ding X Z. Phonon confinement effects in the Raman scattering by TiO_2 nanocrystals. Appl Phys Lett, 1998, **72**: 73–75. DOI: 10.1063/1.120648

[28] Ma W H, Lu Z and Zhang M. Investigation of structural transformations in nanophase titanium dioxide by Raman spectroscopy. Appl Phys A, 1998, **66**: 621–627. DOI: 10.1007/s003390050723

[29] Barborini E, Kholmanov I N, Piseri P, *et al*. Engineering the nanocrystalline structure of TiO_2 films by aerodynamically filtered cluster deposition. Appl Phys Lett, 2002, **81**: 3052–3054. DOI: 10.1063/1.1510579

[30] Swamy V, Kuznetsov A, Dubrovinsky L S, *et al*. Finite-size and pressure effects on the Raman spectrum of nanocrystalline anatase TiO_2. Phys Rev B, 2005, **71**: 184302. DOI: 10.1103/PhysRevB.71.184302

[31] Ohsaka T, Yamaoka S and Shimomura O. Effect of hydrostatic pressure on the Raman spectrum of anatase (TiO_2). Solid State Commun, 1979, **30**: 345–347. DOI:10.1016/0038-1098(79)90648-3

[32] Meng J F, Zou G T, Cui Q L, *et al*. Raman scattering from $PbTiO_3$ of various grain sizes at high hydrostatic pressures. J Phys Condens Matter, 1994, **6**: 6543–6548. DOI:10.1088/0953-8984/6/32/015